Engineering 30 (2023) 121–130

Contents lists available at ScienceDirect

Engineering

journal homepage: www.elsevier.com/locate/eng

Research
Large-Scale Energy Storage—Article

An Integrated Framework for Geothermal Energy Storage with CO_2 Sequestration and Utilization

Yueliang Liu [a,b,c,#], Ting Hu [b,#], Zhenhua Rui [a,b,c,*], Zheng Zhang [b], Kai Du [b], Tao Yang [d], Birol Dindoruk [e], Erling Halfdan Stenby [f], Farshid Torabi [g], Andrey Afanasyev [h]

[a] State Key Laboratory of Petroleum Resources and Prospecting, China University of Petroleum (Beijing), Beijing 102249, China
[b] School of Petroleum Engineering, China University of Petroleum (Beijing), Beijing 102249, China
[c] College of Carbon Neutrality Future Technology, China University of Petroleum (Beijing), Beijing 102249, China
[d] Equinor ASA, Stavanger 4035, Norway
[e] Department of Petroleum Engineering, Cullen College of Engineering, University of Houston, Houston, TX 77204, USA
[f] Center for Energy and Resources Engineering, Department of Chemistry, Technical University of Denmark, Kongens Lyngby 2800, Denmark
[g] Petroleum Systems Engineering, University of Regina, Regina, SK S4S 0A2, Canada
[h] Institute of Mechanics, Moscow State University, Moscow 119192, Russia

ARTICLE INFO

Article history:
Received 13 September 2022
Revised 28 November 2022
Accepted 23 December 2022
Available online 8 March 2023

Keywords:
Geothermal energy storage
CO_2 sequestration
Carbon neutrality
Large-scale
CO_2 utilization

ABSTRACT

Subsurface geothermal energy storage has greater potential than other energy storage strategies in terms of capacity scale and time duration. Carbon dioxide (CO_2) is regarded as a potential medium for energy storage due to its superior thermal properties. Moreover, the use of CO_2 plumes for geothermal energy storage mitigates the greenhouse effect by storing CO_2 in geological bodies. In this work, an integrated framework is proposed for synergistic geothermal energy storage and CO_2 sequestration and utilization. Within this framework, CO_2 is first injected into geothermal layers for energy accumulation. The resultant high-energy CO_2 is then introduced into a target oil reservoir for CO_2 utilization and geothermal energy storage. As a result, CO_2 is sequestrated in the geological oil reservoir body. The results show that, as high-energy CO_2 is injected, the average temperature of the whole target reservoir is greatly increased. With the assistance of geothermal energy, the geological utilization efficiency of CO_2 is higher, resulting in a 10.1% increase in oil displacement efficiency. According to a storage-potential assessment of the simulated CO_2 site, 110 years after the CO_2 injection, the utilization efficiency of the geological body will be as high as 91.2%, and the final injection quantity of the CO_2 in the site will be as high as 9.529×10^8 t. After 1000 years sequestration, the supercritical phase dominates in CO_2 sequestration, followed by the liquid phase and then the mineralized phase. In addition, CO_2 sequestration accounting for dissolution trapping increases significantly due to the presence of residual oil. More importantly, CO_2 exhibits excellent performance in storing geothermal energy on a large scale; for example, the total energy stored in the studied geological body can provide the yearly energy supply for over 3.5×10^7 normal households. Application of this integrated approach holds great significance for large-scale geothermal energy storage and the achievement of carbon neutrality.

© 2023 THE AUTHORS. Published by Elsevier LTD on behalf of Chinese Academy of Engineering and Higher Education Press Limited Company. This is an open access article under the CC BY license (http://creativecommons.org/licenses/by/4.0/).

1. Introduction

The atmospheric concentration of carbon dioxide (CO_2) is increasing sharply due to the acceleration of global industrialization in recent years. This increasing CO_2 concentration is the main cause of climate change and other deleterious impacts on our living environment [1]. According to the International Energy Agency (IEA) report, global energy-related carbon dioxide emissions increased by 6% to 3.63×10^{10} t in 2021 [2]. The absolute increase in global carbon dioxide emissions exceeded 2×10^9 t, the largest increase in history [2].

Since 2000, CO_2 has been used as an excellent working fluid for extracting geothermal energy from deep geothermal layers [3]. Compared with underground brine, CO_2 has three main

* Corresponding author.
E-mail address: zhenhuarui@gmail.com (Z. Rui).
# These authors contributed equally to this work.

https://doi.org/10.1016/j.eng.2022.12.010
2095-8099/© 2023 THE AUTHORS. Published by Elsevier LTD on behalf of Chinese Academy of Engineering and Higher Education Press Limited Company.
This is an open access article under the CC BY license (http://creativecommons.org/licenses/by/4.0/).

superiorities: ① The mineral solubility of CO_2 is smaller than that of formation brine, which reduces pipe or equipment scaling [3]; ② the kinematic viscosity of CO_2 is lower than that of formation brine, which reduces the pressure losses to reservoir rocks [4,5]; and ③ CO_2 is more compressible than liquid water, which allows the generation of a thermosiphon, reducing the strict requirement for circulation pumps [6–9]. It has been found that CO_2 has a higher heat transfer rate than formation brine [10]. However, the geothermal layers have their limited potential for CO_2 storage due to its limited reservoir volume for sequestration [11,12]. Therefore, sedimentary geothermal basins with extremely low permeability caprocks have been proposed for CO_2 storage, as they have been recognized to have large potential for this purpose [13–17]. Recently, the depleted natural gas reservoirs [18] and depleted oil reservoirs [19] was proposed for the suitable sites for CO_2 sequestration and energy storage [20].

Fossil fuel burning generates significant CO_2 emissions, accounting for 73% of global carbon emissions [21]. CO_2 utilization and storage are currently regarded as one of the most feasible and applicable CO_2 capture, utilization, and storage (CCUS) technologies, accounting for 77% of total global carbon reduction to date [22]. One of the most promising methods of CO_2 utilization and storage is to simultaneously use enhanced oil recovery combined with CO_2 sequestration in target reservoirs [23–28]. The performance of CO_2 in enhanced oil recovery greatly relies on the mass transfer between CO_2 and crude oil [29–34]. It has been found that miscibility or near-miscibility achieves higher oil recovery than immiscibility [35–38]. In addition, the CO_2 storage potential is more significant under the condition of miscibility or near-miscibility than under immiscibility [35–38]. To achieve miscibility, the system pressure should be at or above the minimum miscibility pressure (MMP) [39]. However, it is uneconomical to increase the target reservoir pressure artificially to achieve miscibility [40,41]. Recently, chemical solvents such as alcohol, propanol, and dimethyl ether [42,43] have been introduced to accompany CO_2 in enhanced oil recovery, reducing the MMP between CO_2 and crude oil by more than 10%. In addition to reducing the MMP, modified CO_2 injection—such as water alternating gas (WAG) and so forth—has been investigated in order to improve the CO_2 injection performance by increasing the sweep efficiency of CO_2 [44–49].

In this work, we propose an integrated framework for synergistic geothermal energy storage and CO_2 sequestration and utilization. Within this framework, CO_2 is first injected into geothermal layers, where the geothermal energy is efficiently transferred to the low-temperature CO_2 due to the higher heat transfer coefficient of the latter. The resultant high-energy CO_2 is then introduced into the target reservoir for simultaneous CO_2 utilization and sequestration and geothermal energy storage. The schematic work flows of this integrated framework are shown in Fig. 1.

2. Theoretical model

2.1. Overview of simulation tools

In this work, simulations were performed using the TOUGHREACT-EOR code package, which can simulate the interaction between CO_2 and multicomponent oil phases, as well as the multicomponent reactive transport of a complex aqueous phase in subsurface multiphase systems. This simulator has been updated by introducing a multicomponent oil phase to the existing simulation framework of multiphase flow and heat flow with reactive transport [50–52]. For numerical calculations, spatial discretization was carried out using the integral finite difference (IFD), and the time discretization was the fully implicit difference. A sequential iterative approach that referred to a previous work [53] was used in the coupled calculation of flow and reactive transport. Details on the reactive transport simulator are provided in a previous work [54].

The updated oil-bearing multiphase, multicomponent simulation program, coupled with a thermo–hydro–chemical (T–H–C) simulator, still possesses all the merits of the original simulator (i.e., non-isothermal, multiphase solute transport considering convection diffusion, geochemical reactions, and a comprehensive

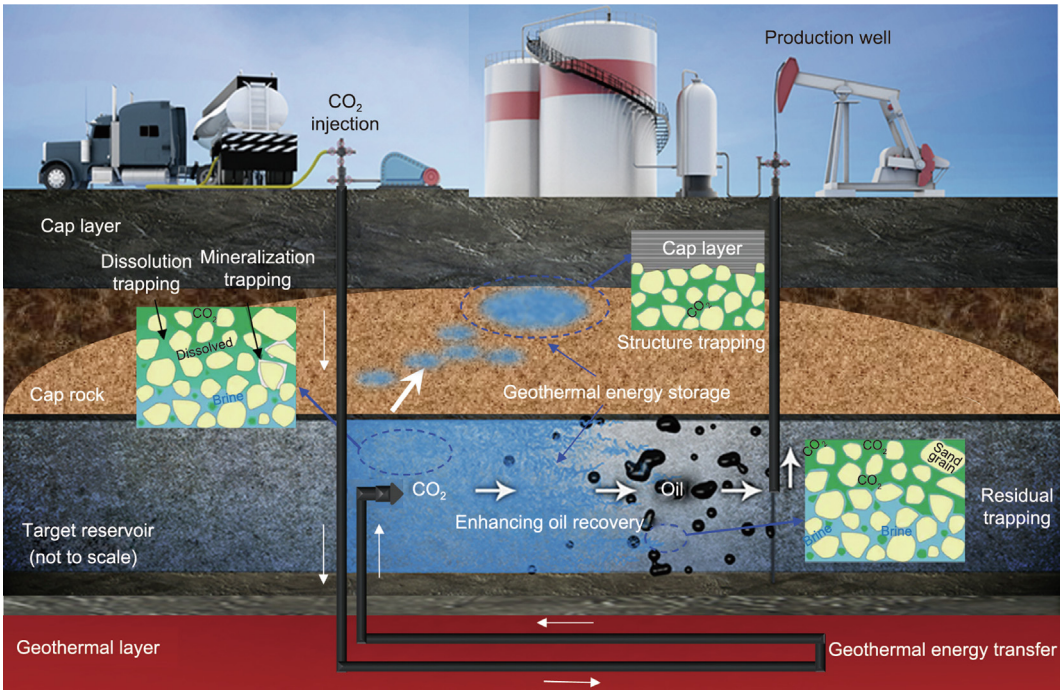

Fig. 1. Schematic work flows of the integrated framework for geothermal energy storage and CO_2 sequestration and utilization.

database of thermodynamic and kinetic parameters). The key differences are that the updated simulator takes into account the following processes: ① flash evaporation to solve the mass transfer process between CO_2 and the multicomponent oil phase; and ② CO_2 miscibility and immiscibility. Overall, the updated simulator can quantitatively characterize the migration and transformation of CO_2 among the supercritical phase, dissolved-in-water phase, dissolved-in-oil phase, and mineralized phase; thus, it is an optional software for carbon sequestration research in CO_2-geological utilization technology.

2.2. Model initial and boundary conditions

In this study, we developed a three-dimensional (3D) wellbore-reservoir coupling model. Fig. 2 presents the longitudinal section of the wellbore-reservoir coupling model, which uses different governing equations to calculate the fluid phase behavior in the wellbore and reservoir. The one-dimensional (1D) two-phase momentum equation is used for the wellbore and the 3D multiphase Darcy's Law is employed for the reservoir [55]. The thickness of the entire stratum is 2.02 km, including a geothermal layer located at the bottom, with a thickness of 100 m and a depth of 3.52 km, and an oil reservoir at the top, with a thickness of 20 m and a depth of 1.5 km. A group of injection-production wells in an inverse "nine-point" well pattern is defined in the model to finish the desired simulation work. Based on the symmetry principle, the 1/4 area of the well pattern is simulated and Dirichlet conditions with fixed temperature and pressure are considered for the lateral boundaries. A semi-analytical solution is used to calculate the heat exchange between the wellbore and formation [56].

Fluids are heated in the geothermal formation through a 200 m horizontal well and then injected into the oil reservoir along a 2.0 km long vertical well. Details of the target reservoir's initial physical parameters and the pseudo components of the crude oil used in our model are provided in Tables 1 and 2 [57], respectively. Details of the geothermal formation's initial physical parameters and the wellbore parameters are presented in Table 3 [58].

The geochemical conditions of the model are set according to the site data. The aqueous solution type is Na–HCO_3, and the stratigraphic lithology is feldspar quartz sandstone. We consider three mechanisms influencing the kinetically controlled mineral dissolution and precipitation, and the reaction rate constant (k) is calculated using the Lasaga model (1984), as shown in Eq. (1):

$$\begin{aligned} k = {} & k_{25}^{\mathrm{nu}} \exp\left[\frac{-E_{\mathrm{a}}^{\mathrm{nu}}}{R}\left(\frac{1}{T_0}-\frac{1}{298.15}\right)\right] \\ & + k_{25}^{\mathrm{H}} \exp\left[\frac{-E_{\mathrm{a}}^{\mathrm{H}}}{R}\left(\frac{1}{T_0}-\frac{1}{298.15}\right)\right] \alpha_{\mathrm{H}}^{n_{\mathrm{H}}} \\ & + k_{25}^{\mathrm{OH}} \exp\left[\frac{-E_{\mathrm{a}}^{\mathrm{OH}}}{R}\left(\frac{1}{T_0}-\frac{1}{298.15}\right)\right] \alpha_{\mathrm{OH}}^{n_{\mathrm{OH}}} \end{aligned} \tag{1}$$

where k_{25} (mol·(m^2·s)$^{-1}$) is the kinetic constant at 25 °C, and E_a (kJ·mol^{-1}) is the activation energy, R is gas constant, T_0 is absolute temperature (K), α is the activity of the species. The power terms (n) for both the acid (H) and base (OH) mechanisms are for H^+, superscripts nu indicate neutral mechanisms. The reaction kinetic parameters related to the geochemical calculation are listed in Tables 4 and 5 [59–61].

The solubilities of the CO_2 and the hydrocarbon component in the gas and oil phases are calculated by flash calculations using the Peng–Robinson (PR) equation of state, and the solubility of the CO_2 in the water phase is calculated using Henry's law. The oil viscosity (μ) in our model is considered to be a function of temperature, pressure, the compression coefficient, and the

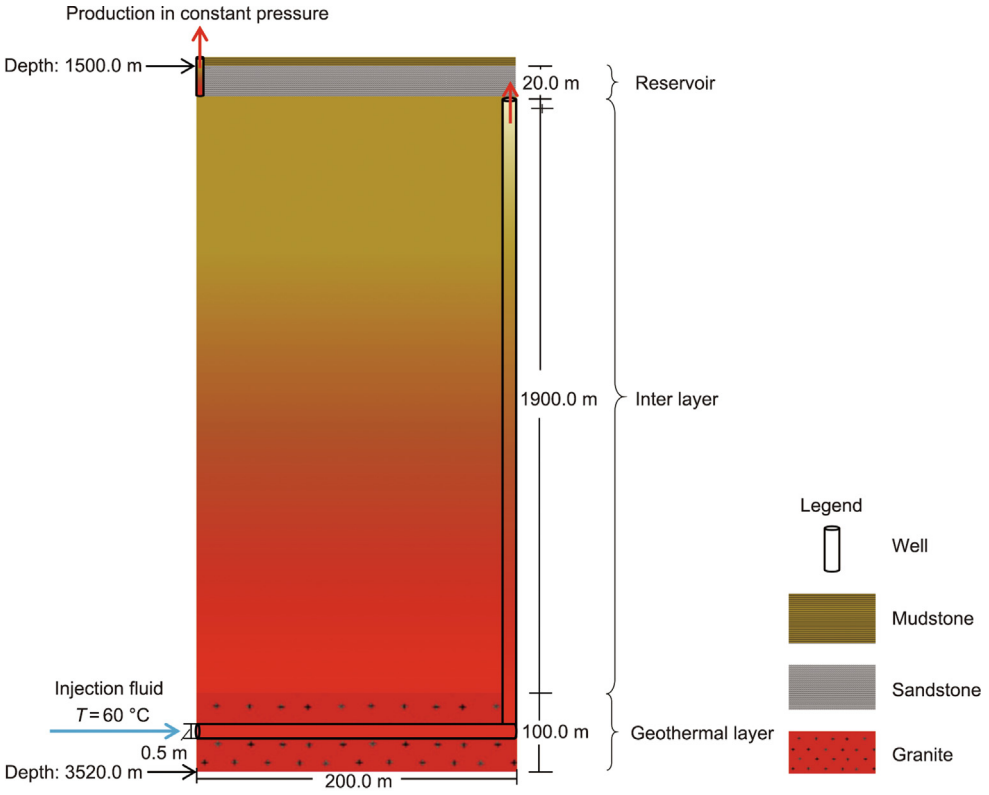

Fig. 2. Longitudinal section of the wellbore-reservoir coupling model.

component properties, taking friction theory into account [62], as shown in Eq. (2):

$$\mu = \frac{1}{f} = \frac{1}{\sum_{i=1}^{N}\sum_{j=1}^{N}\frac{\theta_i\theta_j E_{ij}^{A}}{\sqrt{u_i u_j}}} \tag{2}$$

where f is the fluidity of multicomponent fluids; N is the number of components; u_i and u_j are the viscosity of components i and j, respectively; θ_i (θ_j) is the function of x_i (x_j) and M_i (M_j); and $E_{i,j}^{A}$ is the average efficiency interaction coefficient between component i and j, as shown in Eqs. (3)–(5):

$$\mu_i = \mu_c[1 + a(P - P_c)]\exp(E_a/RT) \tag{3}$$

$$\theta_i = \frac{x_i\sqrt{M_i}}{\sum_{i=1}^{N}x_i M_i} \tag{4}$$

$$E_{i,j}^{A} = \frac{2\sqrt{M_i M_j}}{M_i + M_j} \tag{5}$$

where μ_c is the critical viscosity; T is temperature (K); P is pressure (Pa); a is pressure coefficient (Pa^{-1}); x_i is the molar fraction of component i; and M_i and M_j are the molecular mass of components i and j, respectively.

In this work, the target reservoir is developed by alternately injecting CO_2 and water for 10 years. In the first (i.e., 0–2.5 years) and third (i.e., 5.0–7.5 years) periods of 2.5 years, CO_2 injection is performed. In the second (i.e., 2.5–5.0 years) and fourth (i.e., 7.5–10.0 years) periods of 2.5 years, water injection is performed to improve the sweep volume of the injected fluid and enhance the heat transfer capacity of the geothermal layers. After 10 years of alternating injection cycles, CO_2 is injected continuously for 100 years for CO_2 sequestration and geothermal energy storage; here, it should be noted that geothermal energy is stored in the target geological reservoir body accompanying CO_2 sequestration. Three cases are adopted in this simulation: case 1, in which the CO_2 or water is first injected into the geothermal layers for energy assimilation, and the high-energy CO_2 is then injected into the target geological reservoir body for CO_2 utilization—that is, enhanced oil recovery; case 2, in which CO_2 or water is injected into the target reservoir directly for oil recovery; and case 3, in which the target oil reservoir is assumed to be depleted, and CO_2 is then injected for 100 years for sequestration and, more importantly, geothermal energy is stored in the CO_2 accompanying the CO_2 sequestration.

Table 1
Initial parameters of the target oil reservoir.

Parameter (unit)	Value
Density of the reservoir rock ($kg·m^{-3}$)	2600
Porosity	0.148
Depth of the bottom rock (m)	1500
Permeability (mD)	10.2
Temperature (K)	333.15
Pressure (MPa)	15.0
Heat conduction coefficient of the reservoir rocks ($J·(kg·K)^{-1}$)	2.51
Specific heat capacity of the reservoir rocks ($W·(m·K)^{-1}$)	920
Thickness of reservoir (m)	20.0
Oil saturation	0.51

3. Calculation of energy storage with CO_2

At a given pressure and temperature, the total energy stored in CO_2 is composed of the temperature exergy and the pressure exergy [63], which are given by Eq. (6):

$$e_{x,H} = e_{x,T} + e_{x,P} \tag{6}$$

where $e_{x,H}$ represents the specific enthalpy (i.e., total energy) of CO_2 under given conditions, in $kJ·kg^{-1}$; $e_{x,T}$ represents the specific exergy to temperature, in $kJ·kg^{-1}$; and $e_{x,P}$ represents the specific exergy to pressure, in $kJ·kg^{-1}$.

The $e_{x,P}$ can be considered to be the work done by CO_2 expansion under isothermal conditions, which can be expressed as shown in Eq. (7) [58]:

$$e_{x,P} = e_x(T_s, P_1) - e_x(T_s, P_2) = \int_{P_2}^{P_1} V\mathrm{d}P = T_s R_g \ln\frac{P_1}{P_2} \tag{7}$$

where e_x represents the specific exergy, in $kJ·kg^{-1}$; T_s represents the system temperature, in K; P_1 represents the absolute pressure of CO_2 in the target reservoir, in MPa; P_2 represents the absolute pressure of natural gas at the ground surface, in MPa; V represents the specific volume of CO_2, in $m^3·kg^{-1}$; and R_g represents the gas molar constant.

When the temperature is changed from T_s to the given temperature, the $e_{x,T}$ is calculated as shown in Eq. (8) [64]:

$$\begin{aligned} e_{x,T} &= e_x(T_1, P_1) - e_x(T_s, P_1) = \int_{T_s}^{T} C_P\left(1 - \tfrac{T_s}{T_1}\right)\mathrm{d}T \\ &= C_P(T_s - T_1) - C_P T_s \ln\tfrac{T_s}{T_1} \end{aligned} \tag{8}$$

where T_1 represents the temperature of CO_2, in K; and C_P represents the specific heat capacity at the given pressure, in $kJ·(kg·K)^{-1}$.

4. Results and discussion

4.1. Improved reservoir temperature

The initial temperature of the target reservoir is 333.15 K. The temperature increment of high-energy CO_2/water after flowing through the geothermal layer is expressed as follows (Fig. S1 in Appendix A): During the first 2.5 years, CO_2 is injected through the geothermal layer, which has a temperature of 383.15 K, and is then injected into the target reservoir, which has an initial temperature of 333.15 K. The temperature of the high-energy CO_2

Table 2
Initial pseudo-components of the target reservoir fluid [57].

Component	Mole fraction	P_c (atm[a])	T_c (K)	V_c ($cm^3·mol^{-1}$)	Molecular weight ($g·mol^{-1}$)	Acentric factor
CO_2	0.00970	72.900	304.700	0.094000	44.010	0.225000
N_2 and C_1	0.30880	45.158	189.078	0.089500	16.326	0.013638
C_2	0.03960	48.200	305.430	0.009000	30.070	0.098600
C_3 and C_4	0.04660	40.703	382.490	0.148000	47.589	0.163450
i-C_5 and C_6	0.00170	32.909	470.810	0.203000	73.545	0.248180
C_7–C_{10}	0.05370	26.390	595.870	0.255780	118.180	0.343530
C_{11}–C_{25}	0.16197	19.357	617.830	0.327352	175.470	0.822800
C_{25+}	0.37790	16.922	907.900	0.442394	534.800	1.151000

P_c: the critical pressure; T_c: the critical temperature; V_c: the critical volume; i-C_5: isopentance.
[a] 1 atm = 101325 Pa.

Table 3
List of thermo-physical parameters of the deep geothermal layer.

Parameter (unit)	Value
Density of reservoir rock ($kg·m^{-3}$)	2600
Porosity	0.148
Permeability (mD)	0.101
Depth of bottom rock (m)	3000
Temperature of bottom rock (K)	383.15
Heat conduction coefficient of reservoir rocks ($J·(kg·K)^{-1}$)	2.51
Specific heat capacity of reservoir rocks ($W·(m·K)^{-1}$)	920
Heat conduction coefficient of well wall ($J·(kg·K)^{-1}$)	Horizontal: 4.00, vertical: 0.02
Specific heat capacity of well wall ($W·(m·K)^{-1}$)	750
Diameters of tube (m)	0.5

Table 4
Initial water chemical composition [59].

Component	C ($mol·L^{-1}$)	Component	C ($mol·L^{-1}$)
Na^+	9.25×10^{-2}	SO_4^{2-}	1.09×10^{-2}
K^+	2.88×10^{-2}	HCO_3^-	3.37×10^{-2}
Ca^{2+}	1.26×10^{-3}	Cl^-	1.26×10^{-1}
Mg^{2+}	1.17×10^{-3}	—	—

C: total dissolved concentrations of chemical components, which are concentrations of the basis species plus their associated aqueous secondary species.

(which averages 341.75 K) is always higher than the initial reservoir temperature (333.15 K). To improve the utilization efficiency of the CO_2, its injection is alternated with water injection in the second 2.5-year period. It can be seen that the temperature of the injected water is higher than that of the CO_2, reaching as high as 355.45 K, because the specific heat capacity per unit mass of water is higher than that of CO_2.

In the third period of 2.5 years, high-energy CO_2 is reinjected into the target reservoir. As shown in Fig. S1, the temperature of the high-energy CO_2 decreases sharply at the beginning of the injection. After 2.5 years of water injection, condensate water has filled in the wellbore at the section between the geothermal layer and the target reservoir. When the high-energy CO_2 flows through this section, substantial heat loss occurs due to heat exchange with the condensate water, resulting in an intense decrease in the temperature of the high-energy CO_2. However, the temperature of the high-energy CO_2 gradually increases to around 341.15 K, which is deemed to be beneficial for CO_2 utilization. In the fourth 2.5-year period, water is again injected, this time with an average temperature as high as 351.15 K, which is much higher than the original target reservoir temperature of 333.15 K.

The temperature distributions over the target reservoir during the two cycles of CO_2/water injection are shown in Appendix Fig. S2. The temperature around the injecting wellbore for the high-energy CO_2/water injection is much higher than that of the main body of the target reservoir. Compared with the high-energy CO_2 injection, the high-energy water injection results in a much higher temperature around the injection wellbore. The average temperature of the target reservoir during the 0–2.5-year and 5.0–7.5-year periods of high-energy CO_2 injection is 335.4 and 336.41 K, respectively, which is higher than the initial temperature of the target reservoir. Moreover, the average temperature of the target reservoir during the 2.5–5.0-year and 7.5–10.0-year periods of high-energy water injection is 336.9 and 338.23 K, respectively; thus, the high-energy water injection better promotes the target reservoir temperature than the high-energy CO_2 injection. Compared with injecting CO_2/water directly, the high-energy CO_2/water injection results in the target reservoir having relatively higher temperatures. Higher temperatures enhance the transfer of CO_2 to crude oil and reduce the oil's viscosity, which result in a higher efficiency of CO_2 utilization for enhanced oil recovery. Furthermore, a higher temperature is critical for large-scale geothermal energy storage in CO_2.

4.2. CO_2 geological utilization

Fig. 3 presents the oil viscosity distribution over the target reservoir after 10 years of CO_2/water injection. The oil viscosity is relatively higher near the wellbores than in the main body of the target reservoir. The residual oil near the wellbores is efficiently swept by the CO_2 and injected water, which causes the viscosity to become heavier due to the extraction effect of the CO_2; that is, the CO_2 has a strong extraction effect on the light hydrocarbons in the crude oil. After two cycles of CO_2 extraction, the viscosity of the crude oil increases significantly. The oil viscosity over the whole target reservoir body after cycles of high-energy CO_2/water injection (case 1) is generally smaller than that after injecting CO_2/

Table 5
Initial mineral volume fractions and their kinetic properties [60,61].

Mineral	Vol% of solid	S ($cm^2·g^{-1}$)	Neutral mechanism		Acid mechanism			Base mechanism		
			k_{25} ($mol·(m^2·s)^{-1}$)	E_a ($kJ·mol^{-1}$)	k_{25} ($mol·(m^2·s)^{-1}$	E_a ($kJ·mol^{-1}$)	n (H^+)	k_{25} ($mol·(m^2·s)^{-1}$)	E_a ($kJ·mol^{-1}$)	n (H^+)
Quartz	37.83	9.800	1.140×10^{-8}	87.70	—	—	—	—	—	—
Albite	34.84	483.000	2.750×10^{-13}	69.80	6.920×10^{-11}	65.0	0.457	2.510×10^{-16}	71.0	−0.572
K-feldspar	4.56	9.800	3.891×10^{-13}	38.00	8.710×10^{-11}	51.7	0.500	6.310×10^{-22}	94.1	−0.823
Calcite[a]	2.84	9.800	—	—	—	—	—	—	—	—
Kaolinite	0.12	151.600	6.918×10^{-14}	22.20	4.898×10^{-12}	65.9	0.777	8.913×10^{-18}	17.9	−0.472
Chlorite	0.68	151.600	3.020×10^{-13}	88.00	7.762×10^{-12}	88.0	0.500	—	—	—
Siderite	0.09	9.800	1.260×10^{-9}	62.76	1.590×10^{-4}	45.0	0.900	—	—	—
Na-smectite	6.35	151.600	1.660×10^{-13}	35.00	1.047×10^{-11}	23.6	0.340	3.020×10^{-17}	58.9	−0.400
Ca-smectite	6.35	151.600	1.660×10^{-13}	35.00	1.047×10^{-11}	23.6	0.340	3.020×10^{-17}	58.9	−0.400
Ankerite	3.64	9.800	1.26×10^{-9}	62.76	1.590×10^{-4}	45.0	0.900	—	—	—
Illite	1.70	151.600	1.660×10^{-13}	35.00	1.047×10^{-11}	23.6	0.340	3.020×10^{-17}	58.9	−0.400
Oligoclase	0	19.795	1.445×10^{-12}	69.80	2.138×10^{-10}	65.0	0.457	—	—	—
Magnesite	0	9.800	4.571×10^{-10}	23.50	4.169×10^{-7}	14.4	1.000	—	—	—
Dawsonite	0	9.800	1.260×10^{-9}	62.76	1.590×10^{-4}	45.0	0.900	—	—	—
Dolomite	0	9.800	2.951×10^{-8}	52.20	6.457×10^{-4}	36.1	0.500	—	—	—
Hematite	0	12.900	2.512×10^{-15}	66.20	4.074×10^{-10}	66.2	1.000	—	—	—

Minerals with an initial volume fraction of 0 were secondary components that may have been present during the simulation.
S: the specific reactive surface area per unit mass of solid; vol%: volume percentage of minerals to total rock skeleton.
[a] Calcite is controlled by local equilibrium.

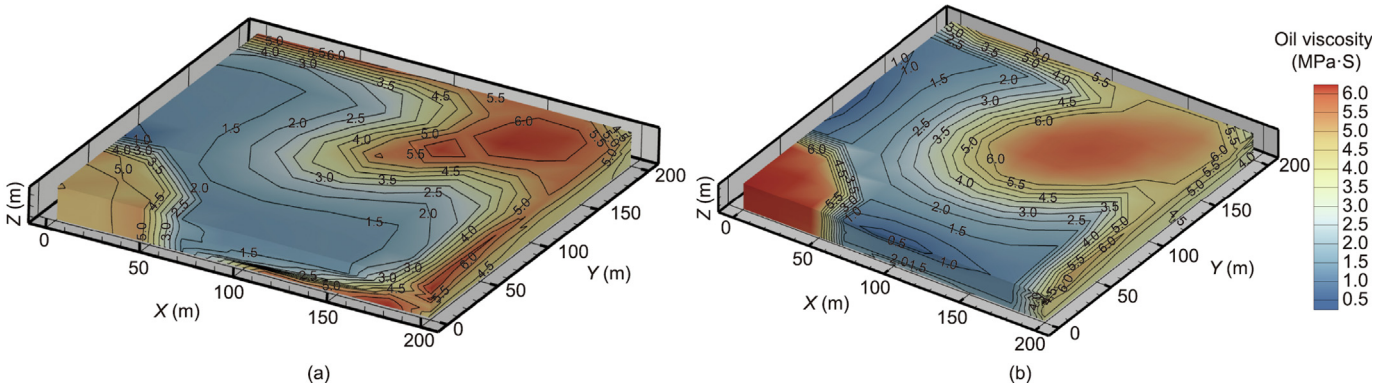

Fig. 3. Oil viscosity distributions over the target reservoir after 10 years of injection: (a) case 1 and (b) case 2.

water directly (case 2). The additional geothermal energy contributes to the viscosity reduction and facilitates CO_2 utilization for enhanced oil recovery.

Fig. 4 presents the oil production in terms of the development time for high-energy CO_2/water injection (case 1) and direct CO_2/water injection (case 2). After the first four years of injection, the oil production is similar in both cases. During the initial development stage, the quantity of CO_2 injected plays the key role in improving CO_2 utilization and sequestration. During the 4th to 10th years of injection, the introduced geothermal energy reduces the oil viscosity and improves the mobility of the crude oil, which favors CO_2 utilization. Without geothermal energy, the injected CO_2/water can readily break through due to the high mobility ratio between the crude oil and the CO_2/water. However, as the mobility ratio decreases over time due to the introduced geothermal energy, the oil production of the direct CO_2/water injection lags behind that of the high-energy CO_2/water injection. In other words, the additional geothermal energy plays a more important role in improving CO_2 utilization during the 4th to 10th years of injection than during the first four years.

When the displacement efficiency in 10 years is calculated according to the sweep volume, the result is 63.6% for case 1 and 53.5% for case 2, as shown in Fig. 4. This result indicates that the main mechanism for enhancing oil recovery in case 1 is the enhanced mass transfer between the CO_2 and the oil due to the high-energy injection. The averaged oil saturation (Fig. S3 in Appendix A) after the high-energy CO_2/water injection is generally lower than that after the direct CO_2/water injection, which validates the higher efficient utilization of CO_2 with the assistance of geothermal energy.

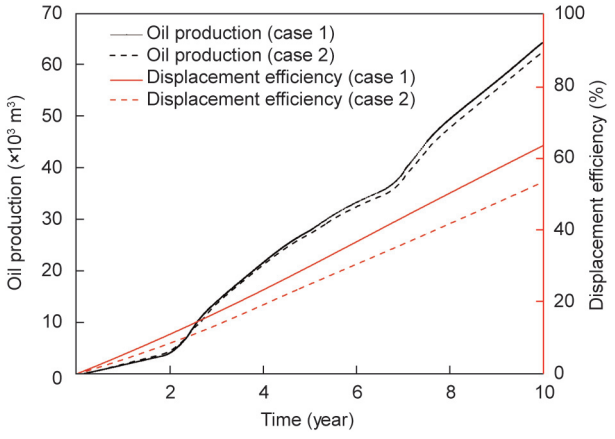

Fig. 4. Oil production and displacement efficiency in terms of development time.

4.3. Energy storage and CO_2 sequestration during oil reservoir development

In the first 2.5 years, a relatively larger amount of CO_2 dissolves into the crude oil as CO_2 is injected continuously (Fig. S4 in Appendix A). As a result, the molar fraction of CO_2 increases, especially near the injection wellbores, with an averaged value of 0.4485. During the 2.5–5.0-year period, water is injected, and the CO_2-saturated reservoir fluids are displaced by the injected water, which results in a sudden decrease in the molar fraction of CO_2. Subsequently, CO_2 is reinjected, and the molar fraction of CO_2 increases to an averaged value of 0.2209, which is less than that during the first round of CO_2 injection. During the 7.5–10-year period, water is again injected, and the molar fraction of CO_2 decreases to an averaged value of 0.1766. As can be seen, the injected water has a major influence on the CO_2 dissolution in the reservoir fluids, which is not beneficial for CO_2 sequestration.

The direct CO_2/water injection (case 2) results in relatively smaller molar fractions of CO_2 in the oil phase (Figs. S4 and S5 in Appendix A). There are two main reasons for this. First, the higher temperatures in the high-energy injection scenario (case 1) keep the viscosity of the reservoir fluids at a relatively low level, which is essential for achieving sufficient contact between the CO_2 and the reservoir fluids. In addition, the CO_2 molecules have a higher diffusion coefficient at higher temperatures, which is critical for the miscibility between the CO_2 and the reservoir fluids. Therefore, the additional geothermal energy is beneficial for CO_2 sequestration in the target reservoirs. The reservoir porosity near the injection wellbore in case 1 is greater than that in case 2 (Fig. S6 in Appendix A). This finding suggests that, with the assistance of geothermal energy, the CO_2/water in case 1 exhibits better performance in flowing and sweeping the residual reservoir fluid out from the target reservoir. The resulting free space in the target reservoir is a suitable site for future large-scale CO_2 sequestration and geothermal energy storage.

CO_2 can also be used as a suitable agent for geothermal energy storage, by transferring deep geothermal energy to a relatively shallow target reservoir for large-scale energy storage. As mentioned previously, the total energy stored in CO_2 is highly dependent on the system pressure and temperature, and is composed of the temperature exergy and the pressure exergy. Fig. S2 presents the average temperature increase of the target reservoir due to the injection of high-energy CO_2/water. The reservoir pressure is greatly increased after injecting high-energy CO_2/water (Fig. S7 in Appendix A); it should be noted here that the original reservoir pressure is 15.0 MPa. The target reservoir presents a lesser pressure increase after the injection of high-energy CO_2/water (case 1) than after the direct CO_2/water injection (case 2). When

geothermal energy is transferred into the target reservoir, the viscosity of the reservoir fluids is significantly reduced, which is beneficial for the dissolution of CO_2 in the reservoir fluids, resulting in a relatively lower reservoir pressure.

In this simulation, CO_2 is injected at 43.2 t per day; after ten years of CO_2/water injection, the total CO_2 injected is 78 840 t, and 5250 t of CO_2 are produced accompanied by reservoir fluids. Thus, for case 1, the effective storage quantity of CO_2 is 68 340 t. Similarly, in case 2, 78 840 t of CO_2 are injected and the quantity of CO_2 produced is 6750 t. Thus, for case 2, the effective storage quantity of CO_2 is 65 340 t. According to Eq. (3), the geothermal energy stored in the CO_2 in case 1 can be calculated to be around 2.10×10^4 GJ. (The CO_2 in case 2 is not considered to store geothermal energy in this work.) In order to improve the storage capacity of geothermal energy and CO_2 sequestration in the target geological reservoir body, the target oil reservoir is deemed to be depleted at this point, and five more injection wells are built for CO_2 injection (Section 4.4).

4.4. Energy storage and CO_2 sequestration in a geological oil reservoir body

Based on the geological background of Block H59 in Jilin Oilfield, China [40], a 1:1 3D numerical model was established, as shown in Fig. 5. According to the existing well deployment, six injection wells are opened for CO_2 injection in the model. This model is employed to assess the potential of the site sequestration and energy storage capacity of CO_2. The heat extraction rate gradually decreases as the injection time increases (Fig. S8 in Appendix A), indicating that, as more CO_2 is injected into the target reservoir over time, the temperature of the CO_2 decreases. Therefore, the heat extraction process is stopped after 30 years of CO_2 injection through the geothermal layer, considering the low efficiency of heat extraction. After 30 years, CO_2 is injected directly into the target oil reservoir for another 80 years for CO_2 sequestration.

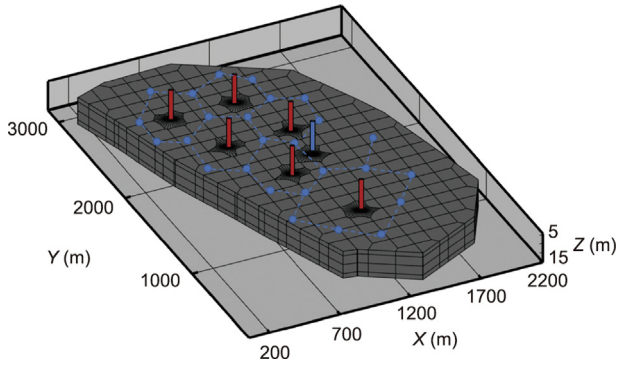

Fig. 5. Concept model of the oil reservoir site for sequestration and energy storage-potential assessment.

After 10 years of oil reservoir development (i.e., water injection alternating with CO_2 injection), CO_2 is then injected for 100 years for CO_2 sequestration and energy storage, until more than 90% of the total porosity of the entire site is occupied. Fig. 6 presents the spatial distribution of the CO_2 after 110 years at different reservoir depths. Due to its buoyancy, CO_2 accumulates in large quantities at the top of the oil reservoir geological body. In order to improve the utilization efficiency of the oil reservoir geological body, six injection wells are opened for CO_2 injection after 10 years' oil production. Fig. 7 presents the utilization efficiency of the reservoir geological body and the corresponding total quantity of CO_2 injection. It is found that the utilization efficiency of the geological body increases as more CO_2 is injected. The final quantity of CO_2 injection at the site is as high as 9.529×10^8 t, at which the utilization efficiency of the geological body is up to 91.2%.

In addition to CO_2 sequestration, the CO_2 is employed as an excellent medium for geothermal energy storage. According to Eq. (3), the total energy stored in the target geological reservoir body is calculated in terms of the injection time. Fig. 8 presents the geothermal energy stored in the target geological reservoir body as CO_2 is injected. It can be seen that the energy stored is transformed into a standard coal mass in Fig. 8. The calorific value of standard coal is 2.933×10^4 kJ·kg^{-1}, which is a method for representing standard energy. We find that the geothermal energy stored by CO_2 increases linearly as more CO_2 is injected and sequestrated in the target geological reservoir body. The geothermal energy stored through CO_2 is as much as 2.46×10^8 GJ after 100 years of CO_2 injection. If it is assumed that the general energy consumption of a normal household is around 7.0 GJ·a^{-1}, then the energy stored through CO_2 could provide the yearly energy supply for over 3.5×10^7 normal households. Therefore, a substantial amount of geothermal energy stored through CO_2 can be meaningful for a future energy supply. In addition, the integrated approach well combines geothermal energy storage with CO_2 sequestration and utilization, and its wide application holds great significance for both large-scale geothermal energy storage and the achievement of future carbon neutrality goals.

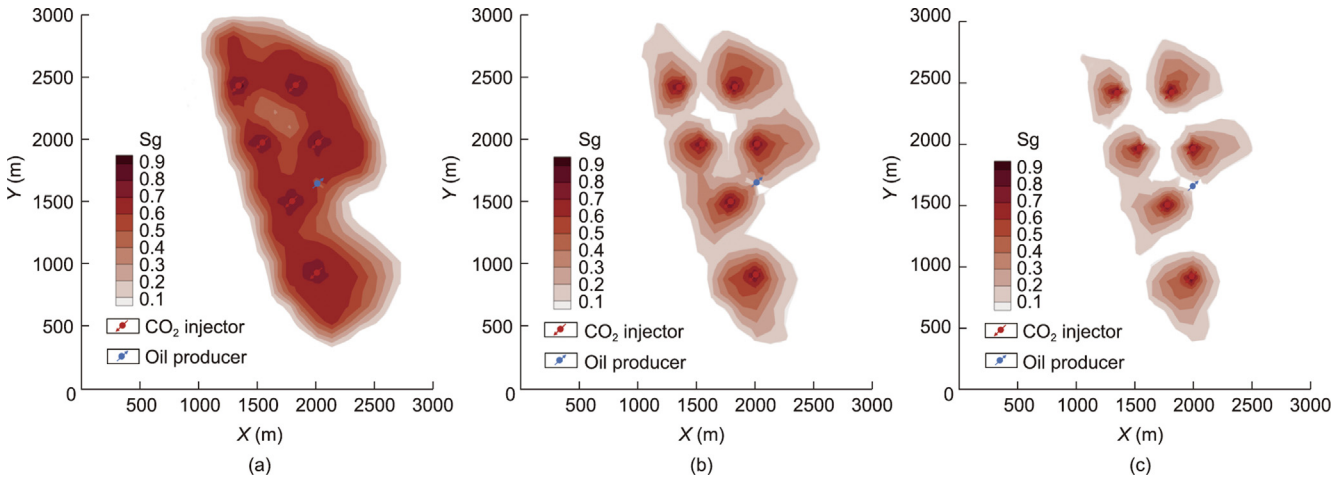

Fig. 6. Spatial distribution of CO_2 in 110 years at different reservoir depths. (a) −1500 m; (b) −1505 m; (c) −1520 m. Sg: the saturation of CO_2.

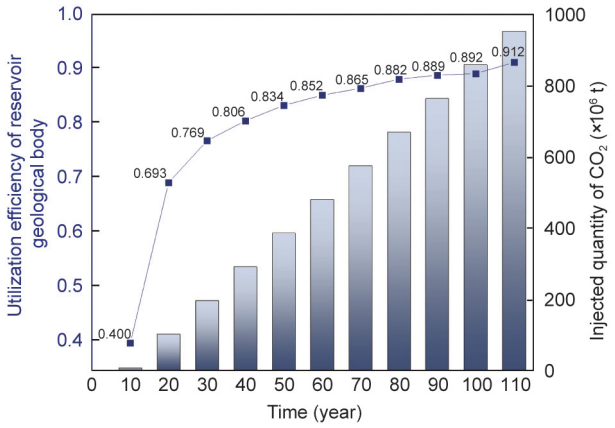

Fig. 7. Utilization efficiency of the reservoir geological body and its corresponding total quantity of CO_2 injection.

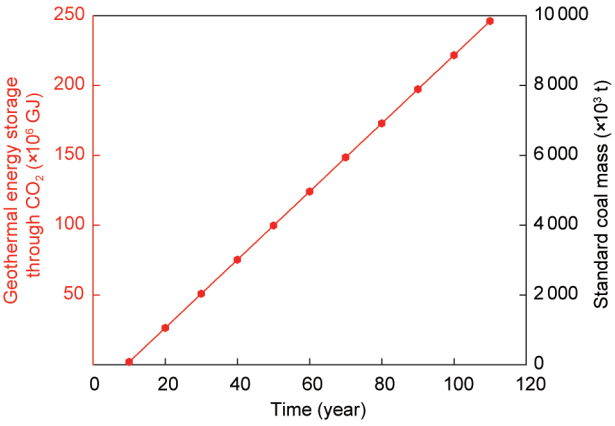

Fig. 8. Geothermal energy stored in the target geological reservoir body as CO_2 is injected.

In order to evaluate the security of CO_2 sequestration in the target geological oil reservoir body, we quantitatively investigated the phase transitions of CO_2 in the next 1000 years when sequestrated in the target reservoir, as shown in Fig. 9. More specifically, the proportion of CO_2 in each phase—that is, the CO_2 dissolved in the oil phase, water phase, gas phase (supercritical), and mineralized phase—is calculated in terms of the sequestrated time. The CO_2 in the target oil reservoir body mainly exists as supercritical CO_2, accounting for up to 70% of the total CO_2; this is followed in order by CO_2 in the liquid phase and then CO_2 in the mineralized phase. The amount of CO_2 dissolved in the oil phase is greater than that in the water phase; in other words, in the geological oil reservoir body, CO_2 tends to dissolve into the oil phase rather than the water phase for sequestration. As the sequestration process continues, the quantity of CO_2 dissolved in the aqueous phase increases as the CO_2 is further transformed into carbonate minerals, of which there are up to around 7.2×10^5 t after 1000 years' sequestration. Thus, the total amount of gaseous CO_2 decreases. In comparison, the total amount of CO_2 dissolved in the oil phase remains basically unchanged.

5. Conclusions

This work proposed an integrated framework for synergistic geothermal energy storage, carbon sequestration, and CO_2 utilization. The key conclusions are summarized as follows:

(1) When injected through the geothermal layer, CO_2 is heated to an average temperature of 341.75 K. After the injection of high-energy CO_2 for 2.5 years, the average temperatures of the target reservoir increase by around 276.15 K, and the average pressure of the target reservoir increases to 25.1–47.7 MPa, which is beneficial for efficient CO_2 utilization and geothermal energy storage.

(2) By introducing geothermal energy into the target reservoir, the solubility of CO_2 in the reservoir fluids is greatly improved. The injection of high-energy CO_2/water exhibits a better performance

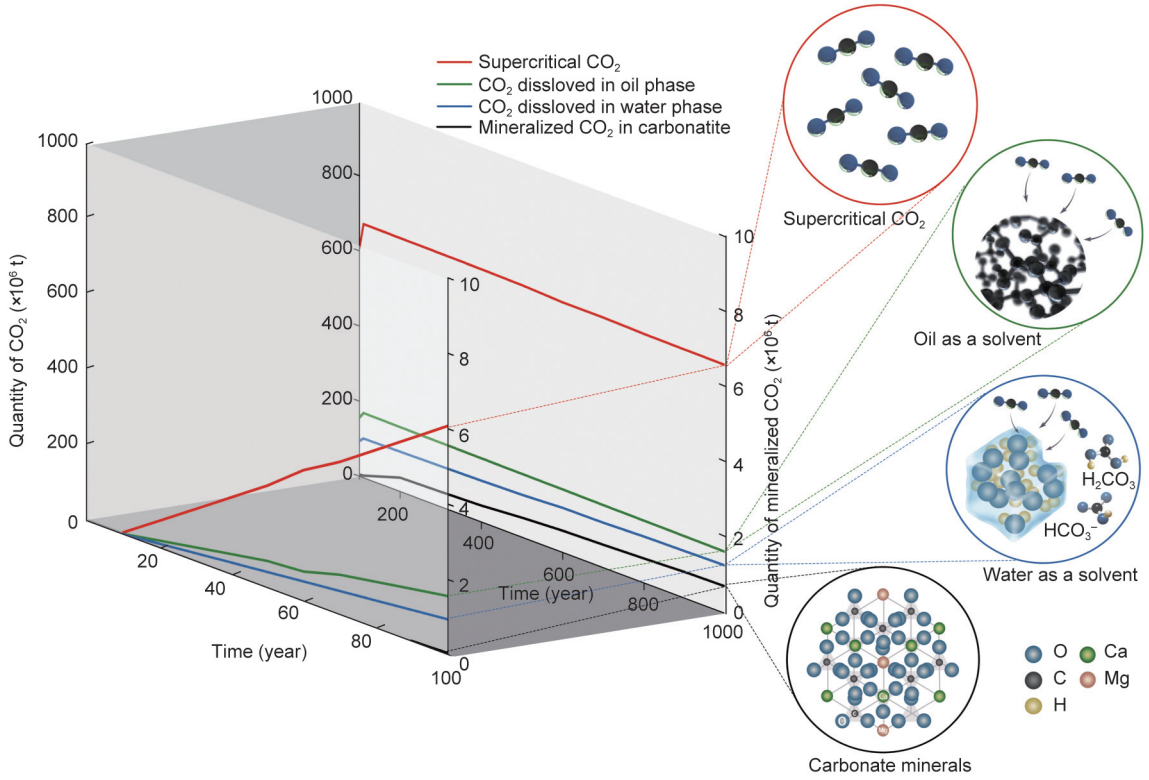

Fig. 9. Phase transitions of CO_2 in the target geological reservoir body over the next 1000 years.

than the direct injection of CO_2/water in sweeping the reservoir fluids out from the pore and throat, due to the introduction of the geothermal energy. Hence, the free space in the target reservoir becomes a suitable site for future large-scale CO_2 sequestration and geothermal energy storage.

(3) When CO_2 is injected for 110 years, the utilization efficiency of the geological body reaches 91.2% and the final injection quantity of CO_2 in the site is as high as 9.529×10^8 t. After 1000 years of sequestration, CO_2 mainly exists in the form of supercritical CO_2, which accounts for up to 70% of the total CO_2; this is followed in order by CO_2 in the liquid phase and then CO_2 in the mineralized phase. Moreover, the amount of CO_2 dissolved in the oil phase is greater than that in the water phase; in other words, CO_2 sequestration accounting for dissolution trapping increases significantly due to the presence of residual oil.

(4) CO_2 can be employed as a suitable medium for geothermal energy storage, as it can extract heat from deep geothermal layers and then be used to efficiently store the extracted heat in the target reservoir. As much as 2.46×10^8 GJ of geothermal energy can be stored in the CO_2 after 100 years of CO_2 injection, which could provide a yearly energy supply for over 35×10^6 normal households. This degree of large-scale energy storage is of great significance for providing a future large-scale supply of geothermal energy.

(5) The integrated approach synergistically combines geothermal energy storage with CO_2 sequestration and utilization, which is of great significance for large-scale geothermal energy storage in the future; in addition, the combined approach is beneficial for achieving the goal of carbon neutrality.

Acknowledgments

This work is supported by the National Key Research and Development Program of China under grant (2022YFE0206700). We also acknowledge the financial support by the National Natural Science Foundation of China (52004320), and the Science Foundation of China University of Petroleum, Beijing (2462021QNXZ012 and 2462021YJRC012).

Compliance with ethics guidelines

Yueliang Liu, Ting Hu, Zhenhua Rui, Zheng Zhang, Kai Du, Tao Yang, Birol Dindoruk, Erling Halfdan Stenby, Farshid Torabi, and Andrey Afanasyev declare that they have no conflict of interest or financial conflicts to disclose.

Appendix A. Supplementary data

Supplementary data to this article can be found online at https://doi.org/10.1016/j.eng.2022.12.010.

References

[1] Goeppert A, Czaun M, May RB, Prakash GKS, Olah GA, Narayanan SR. Carbon dioxide capture from the air using a polyamine based regenerable solid adsorbent. J Am Chem Soc 2011;133(50):20164–7.
[2] International Energy Agency (IEA). Global energy review: CO_2 emissions in 2021. Report. Paris: International Energy Agency; 2021.
[3] Brown DW. A hot dry rock geothermal energy concept utilizing supercritical CO_2 instead of water. In: Proceedings of the Twenty-Fifth Workshop on Geothermal Reservoir Engineering; 2000 Jan 24–26; Stanford, CA, USA. Stanford: Stanford Geothermal Program Workshop; 2000. p. 1–6.
[4] Pruess K. Enhanced geothermal systems (EGS) using CO_2 as working fluid—a novel approach for generating renewable energy with simultaneous sequestration of carbon. Geothermics 2006;35(4):351–67.
[5] Pruess K. On production behavior of enhanced geothermal systems with CO_2 as working fluid. Energy Convers Manage 2008;49(6):1446–54.
[6] Atrens AD, Gurgenci H, Rudolph V. CO_2 thermosiphon for competitive geothermal power generation. Energy Fuels 2009;23(1):553–7.
[7] Atrens AD, Gurgenci H, Rudolph V. Electricity generation using a carbon-dioxide thermosiphon. Geothermics 2010;39(2):161–9.
[8] Adams BM, Kuehn TH, Bielicki JM, Randolph JB, Saar MO. A comparison of electric power output of CO_2 plume geothermal (CPG) and brine geothermal systems for varying reservoir conditions. Appl Energy 2015;140:365–77.
[9] Randolph JB, Adams BM, Kuehn TH, Saar MO. Wellbore heat transfer in CO_2-based geothermal systems. Trans Geotherm Resour Coun 2012;36:546–54.
[10] Pruess K. Enhanced geothermal systems (EGS): comparing water and CO_2 as heat transmission fluids. In: Proceedings of the New Zealand Geothermal Workshop; 2006 Nov 28; Auckland, New Zealand. Auckland: Geothermal Association; 2007. p. 1–13.
[11] Randolph JB, Saar MO. Combining geothermal energy capture with geologic carbon dioxide sequestration. Geophys Res Lett 2011;38(10):L10401.
[12] Randolph JB, Saar MO. Impact of reservoir permeability on the choice of subsurface geothermal heat exchange fluid: CO_2 versus water and native brine. Trans Geotherm Resour Counc 2011;35:521–6.
[13] Liu Y, Hou J. Selective adsorption of CO_2/CH_4 mixture on clay-rich shale using molecular simulations. J CO_2 Util 2020;39:101143.
[14] Bielicki JM, Pollak MF, Fitts JP, Peters CA, Wilson EJ. Causes and financial consequences of geologic CO_2 storage reservoir leakage and interference with other subsurface resources. Int J Greenh Gas Control 2014;20:272–84.
[15] Bielicki JM, Peters CA, Fitts JP, Wilson EJ. An examination of geologic carbon sequestration policies in the context of leakage potential. Int J Greenh Gas Control 2015;37:61–75.
[16] Bielicki JM, Pollak MF, Deng H, Wilson EJ, Fitts JP, Peters CA. The leakage risk monetization model for geologic CO_2 storage. Environ Sci Technol 2016;50(10):4923–31.
[17] Gibbins J, Chalmers H. Carbon capture and storage. Energy Policy 2008;36(12):4317–22.
[18] Ezekiel J, Ebigbo A, Adams BM, Saar MO. Combining natural gas recovery and CO_2-based geothermal energy extraction for electric power generation. Appl Energy 2020;269:115012.
[19] Hefny M, Qin CZ, Saar MO, Ebigbo A. Synchrotron-based pore-network modeling of two-phase flow in Nubian Sandstone and implications for capillary trapping of carbon dioxide. Int J Greenh Gas Control 2020;103:103164.
[20] Fleming MR, Adams BM, Ogland-Hand JD, Bielicki JM, Kuehn TH, Saar MO. Flexible CO_2-plume geothermal (CPG-F): using geologically stored CO_2 to provide dispatchable power and energy storage. Energy Convers Manage 2022;253:115082.
[21] Intergovernmental Panel on Climate Change (IPCC). Special report on carbon dioxide capture and storage. Report. Cambridge: Cambridge University Press; 2005.
[22] Presser D, Cafaro VG, Cafaro D. Optimal sourcing, supply and development of carbon dioxide networks for enhanced oil recovery in CCUS systems. Computer-Aided Chem Eng 2022;49:493–8.
[23] Ampomah W, Balch RS, Cather M, Will R, Gunda D, Dai Z, et al. Optimum design of CO_2 storage and oil recovery under geological uncertainty. Appl Energy 2017;195:80–92.
[24] Jia W, McPherson B, Pan F, Dai Z, Xiao T. Uncertainty quantification of CO_2 storage using Bayesian model averaging and polynomial chaos expansion. Int J Greenh Gas Control 2018;71:104–15.
[25] Keating E, Bacon D, Carroll S, Mansoor K, Sun Y, Zheng L, et al. Applicability of aquifer impact models to support decisions at CO_2 sequestration sites. Int J Greenh Gas Control 2016;52:319–30.
[26] Jiang J, Rui Z, Hazlett R, Lu J. An integrated technical-economic model for evaluating CO_2 enhanced oil recovery development. Appl Energy 2019;247:190–211.
[27] Chaturvedi KR, Sharma T. *In-situ* formulation of pickering CO_2 foam for enhanced oil recovery and improved carbon storage in sandstone formation. Chem Eng Sci 2021;235:116484.
[28] Rezk MG, Foroozesh J, Zivar D, Mumtaz M. CO_2 storage potential during CO_2 enhanced oil recovery in sandstone reservoirs. J Nat Gas Sci Eng 2019;66:233–43.
[29] Gu Y, Zhang S, She Y. Effects of polymers as direct CO_2 thickeners on the mutual interactions between a light crude oil and CO_2. J Polym Res 2013;20(2):61.
[30] Pan F, McPherson BJ, Dai Z, Jia W, Lee SY, Ampomah W, et al. Uncertainty analysis of carbon sequestration in an active CO_2-EOR field. Int J Greenh Gas Control 2016;51:18–28.
[31] Davarpanah A, Mirshekari B. Experimental study of CO_2 solubility on the oil recovery enhancement of heavy oil reservoirs. J Therm Anal Calorim 2020;139(2):1161–9.
[32] Liu Y, Li H, Okuno R. Measurements and modeling of interfacial tension of CO_2–CH_4–brine system at reservoir conditions. Ind Eng Chem Res 2016;55(48):12358–75.
[33] Kong S, Feng G, Liu Y, Li K. Potential of dimethyl ether as an additive in CO_2 for shale oil recovery. Fuel 2021;296:120643.
[34] Huang X, Li A, Li X, Liu Y. Influence of typical core minerals on tight oil recovery during CO_2 flooding using the nuclear magnetic resonance technique. Energy Fuels 2019;33(8):7147–54.
[35] Azzolina NA, Nakles DV, Gorecki CD, Peck WD, Ayash SC, Melzer LS, et al. CO_2 storage associated with CO_2 enhanced oil recovery: a statistical analysis of historical operations. Int J Greenh Gas Control 2015;37:384–97.
[36] Aminu MD, Nabavi SA, Rochelle CA, Manovic V. A review of developments in carbon dioxide storage. Appl Energy 2017;208:1389–419.
[37] Bachu S. Identification of oil reservoirs suitable for CO_2-EOR and CO_2 storage (CCUS) using reserves databases, with application to Alberta, Canada. Int J Greenh Gas Control 2016;44:152–65.

[38] Yang W, Peng B, Liu Q, Wang S, Dong Y, Lai Y. Evaluation of CO_2 enhanced oil recovery and CO_2 storage potential in oil reservoirs of Bohai Bay Basin. China Int J Greenh Gas Control 2017;65:86–98.
[39] Ahmed T. Minimum miscibility pressure from EOS. In: Proceedings of Canadian International Petroleum Conference; 2000 Jun 4–8; Calgary, AB, Canada. Calgary: Petroleum Society of Canada; 2000.
[40] Ren B, Ren S, Zhang L, Chen G, Zhang H. Monitoring on CO_2 migration in a tight oil reservoir during CCS-EOR in Jilin Oilfield China. Energy 2016;98:108–21.
[41] Rommerskirchen R, Nijssen P, Bilgili H, Sottmann T. Additives for CO_2 EOR applications. In: Proceedings of Annual Technical Conference and Exhibition (ACTE); 2016 Sep 26–28; Dubai, United Arab Emirates. Dubai: Society of Petroleum Engineers; 2016.
[42] Liu Y, Rui Z. A storage-driven CO_2 EOR for net-zero emission target. Engineering 2022;18(11):79–87.
[43] Liu Y, Rui Z, Yang T, Dindoruk B. Using propanol as an additive to CO_2 for improving CO_2 utilization and storage in oil reservoirs. Appl Energy 2022;311:118640.
[44] Salehi MM, Safarzadeh MA, Sahraei E, Nejad SAT. Comparison of oil removal in surfactant alternating gas with water alternating gas, water flooding and gas flooding in secondary oil recovery process. J Petrol Sci Eng 2014;120:86–93.
[45] Dai Z, Middleton R, Viswanathan H, Fessenden-Rahn J, Bauman J, Pawar R, et al. An integrated framework for optimizing CO_2 sequestration and enhanced oil recovery. Environ Sci Technol Lett 2014;1(1):49–54.
[46] Adebayo AR, Kamal MS, Barri AA. An experimental study of gas sequestration efficiency using water alternating gas and surfactant alternating gas methods. J Nat Gas Sci Eng 2017;42:23–30.
[47] Zhao X, Liao X, Wang W, Chen C, Liao C, Rui Z. Estimation of CO_2 storage capacity in oil reservoir after waterflooding: case studies in Xinjiang Oilfield from west China. Adv Mat Res 2013;734–7:1183–8.
[48] Zhao X, Liao X, Wang W, Chen C, Rui Z, Wang H. The CO_2 storage capacity evaluation: methodology and determination of key factors. J Energy Inst 2014;87(4):297–305.
[49] Zhao X, Rui Z, Liao X. Case studies on the CO_2 storage and EOR. In heterogeneous, highly water-saturated, and extra-low permeability Chinese reservoir. J Nat Gas Sci Eng 2016;29:275–83.
[50] Xu T, Li J. Reactive transport modeling to address the issue of CO_2 geological sequestration. Procedia Earth Planet Sci 2013;7:912–5.
[51] Xu T, Apps JA, Pruess K. Numerical simulation of CO_2 disposal by mineral trapping in deep aquifers. Appl Geochem 2004;19(6):917–36.
[52] Oldenburg CM, Pan L. TOGA: A TOUGH code for modeling three-phase, multicomponent, and non-isothermal processes involved in CO_2-based enhanced oil recovery. Report. Berkeley: Lawrence Berkeley National Laboratory; 2019.
[53] Yeh G, Tripathi S. A model for simulating transport of reactive multispecies components: model development and demonstration. Water Resour Res 1991;27(12):3075–94.
[54] Hu T. Study on the process model of CO_2 migration and phase transformation in enhanced oil recovery system [dissertation]. Changchun: Jilin University; 2022. Chinese.
[55] Pan L, Oldenburg CM. T2Well—an integrated wellbore-reservoir simulator. Comput Geosci 2014;65:46–55.
[56] Ramey HJ. Wellbore heat transmission. J Pet Technol 1962;14(04):427–35.
[57] Guo X, Du Z, Sun L, Fu Y, Huang W, Zhang C. Optimization of tertiary water-alternate-CO_2 flood in Jilin oil field of China: laboratory and simulation studies. In: Proceedings of SPE/DOE Symposium on Improved Oil Recovery; 2006 Apr 22–26; Tulsa, OK, USA. Richardson: OnePetro; 2006. p. SPE-99616-MS.
[58] Hu Z, Xu T, Feng B, Yuan Y, Li F, Feng G, et al. Thermal and fluid processes in a closed-loop geothermal system using CO_2 as a working fluid. Renew Energy 2020;154:351–67.
[59] Lei H. Deposition mechanisms and reservoir protection countermeasures of a low-permeability formation in CO_2 flooding process [dissertation]. Beijing: China University of Petroleum; 2017. Chinese.
[60] Zhang L, Li X, Ren B, Cui G, Zhang Y, Ren S, et al. CO_2 storage potential and trapping mechanisms in the H-59 block of Jilin Oilfield China. Int J Greenh Gas Control 2016;49:267–80.
[61] Tian H, Pan F, Xu T, McPherson BJ, Yue G, Mandalaparty P. Impacts of hydrological heterogeneities on caprock mineral alteration and containment of CO_2 in geological storage sites. Int J Greenh Gas Control 2014;24:30–42.
[62] Quiñones-Cisneros SE, Zéberg-Mikkelsen CK, Stenby EH. The friction theory (f-theory) for viscosity modeling. Fluid Phase Equilib 2000;169(2):249–76.
[63] Aprhornratana S, Eames IW. Thermodynamic analysis of absorption refrigeration cycles using the second law of thermodynamics method. Int J Refrig 1995;18(4):244–52.
[64] Vidal A, Best R, Rivero R, Cervantes J. Analysis of a combined power and refrigeration cycle by the exergy method. Energy 2006;31(15):3401–14.